Astronomy & Astrophysics

Deficit of primitive compositions in binary asteroids and pairs[*]

K. Minker[1,2] and B. Carry[2]

[1] Université Côte d'Azur, Observatoire de la Côte d'Azur, CNRS, Laboratoire Lagrange, Bd de l'Observatoire, CS 34229, 06304 Nice Cedex 4, France
e-mail: kate.minker@oca.eu
[2] MAUCA – Master track in Astrophysics, Université Côte d'Azur & Observatoire de la Côte d'Azur, Parc Valrose, 06100 Nice, France

ABSTRACT

Context. Small binary asteroid systems and pairs are thought to form through fission induced by spin up via the Yarkovsky-O'Keefe-Radzievskii-Paddack (YORP) effect. This process is expected to depend on their structural strength and therefore composition.
Aims. We aim to determine how taxonomic classes – used as a proxy for composition – are distributed amongst binary asteroids and asteroid pairs compared to the general population.
Methods. We compared the distribution of taxonomic classes of binary systems and pairs with that of a reference sample of asteroids. We built this sample by selecting asteroids in a way that reproduces the orbital and size distribution of the binaries and pairs. We did this in order to minimize potential biases between samples.
Results. A strong deficit of primitive compositions (C, B, P, D types) among binary asteroids and asteroid pairs is identified, as well as a strong excess of asteroids with mafic-silicate-rich surface compositions (S, Q, V, A types).
Conclusions. Amongst low-mass, rapidly rotating asteroids, those with mafic-silicate-rich compositions are more likely to form multiple asteroid systems than their primitive counterparts.

Key words. minor planets, asteroids: general – methods: statistical

1. Introduction

Binary systems have long been of interest to astronomers, as a closely orbiting companion can reveal the mass and subsequently the density the primary object. This is true for all varieties of celestial objects, including stars (Herchel 1832; Hadley 1903), exoplanetary systems (Bracewell & MacPhie 1979), and even black holes (Gibbons 1971). Of course, asteroids pose no exception to this rule, and the possible discovery of asteroids with companions has been discussed since the early 20th century (Weidenschilling et al. 1989). Once the existence of these systems was confirmed with the discovery of Dactyl around (243) Ida in 1993 (Chapman et al. 1995), the detection and characterization of binary asteroid systems, also known as asteroids with satellites, has been a significant point of interest for observers.

Several general populations of binary systems are observed. Many of the earliest identified binaries were large ($D_p > 100$ km) main-belt asteroids with small satellites (Merline et al. 2002). A similar population is observed within the Kuiper Belt, alongside a population of large binary systems with two similarly sized components (Fraser et al. 2017). The largest population of known binary systems is composed of small asteroids in the inner Solar System with small satellites; these are the focus of the present study.

As of January 10, 2023, at least 402 binary systems have been identified, and an estimated $15 \pm 4\%$ of the near-Earth asteroids (NEAs) are expected to be in binary systems (Pravec et al. 2006; Margot et al. 2015), as are a significant fraction of main-belt asteroids. A substantial portion of all known binary asteroid systems share highly similar properties, containing rapidly rotating primaries with spin periods close to the stability limit of 2.4 h, an obliquity approaching 0° or 180°, a secondary to primary diameter ratio of $d_s/d_p \approx 0.3$, a primary diameter of less than 15 km, and a 2:1 relationship between the system semi-major axis and the primary diameter, as can be seen in Fig. 1 (or Margot et al. 2015, for a review). These objects are found throughout the inner Solar System and account for over 80% of the known binary asteroid systems; they do not include Kuiper Belt objects (KBOs).

These binary systems are expected to be produced by a common formation mechanism, a rotational-fission model proposed by Walsh et al. (2008), with variations proposed by Jacobson & Scheeres (2011) and Jacobson et al. (2014). The compositional idiosyncrasies of this population of small, rapidly rotating binary systems are not well studied, but early models by Walsh et al. (2008) suggest that dark taxonomic types would be more likely to form binary systems as a result of their higher porosity. An observational study by Pajuelo et al. (2018) found a deficit of C-type NEA binaries, but agreement for all other types with the general population within a 1σ uncertainty. More recently, simulations of the structural evolution of asteroids such as Ryugu and Bennu, targets of the Hayabusa and OSIRIS-REx missions (Fujiwara et al. 2006; Hamilton et al. 2019), suggest that dark taxonomic types may, on the contrary, be less likely to form binary systems at high spin rates, as they undergo structural deformation rather than rotational fission under these circumstances (Zhang et al. 2022).

We aim here to establish whether the distribution of taxonomic classes amongst binary systems is similar to or different
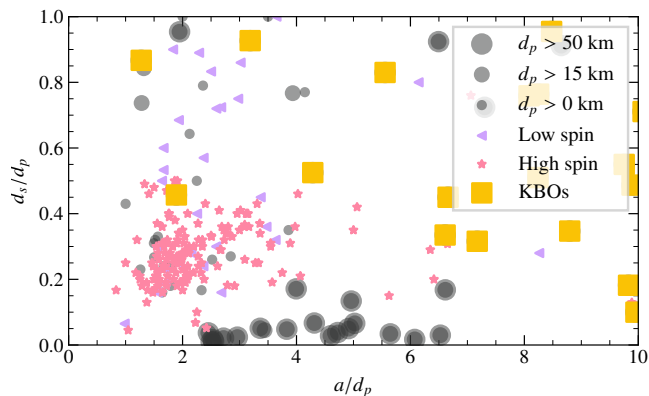

Fig. 1. Known binary systems in the Solar System, including asteroids and KBOs. "Low spin" and "High spin" objects indicated by stars and triangles, respectively, are those that have been considered in this study (objects with $D < 15$ km and $a < 2.502$ au). "High spin" objects have a primary rotation period of less than 4 h, and "Low spin" objects have primary rotation periods of greater than 4 h. The diameters of objects that are not included in the study are indicated by marker size and separated into three sets of $d_p > 50$ km, 50 km $> d_p > 15$ km, and $d_p < 15$ km. Diameters d_s, d_p, and the system semi-major a are in kilometers (km).

than that of the general asteroid population. In Sect. 2, we present the data used in this study and the sources from which they were acquired. In Sect. 3, we discuss how we build a taxonomic reference by selecting asteroids from the general population. In Sect. 4, we show the resulting discrepancies in composition between the binary systems and general population. Section 5 provides a discussion of these results.

2. Datasets

In this study, three main populations were considered. First, the 402 known binary asteroids. Second, asteroid pairs, which are expected to have originated as binary systems that are no longer gravitationally bound (Vokrouhlický & Nesvorný 2008). There are 239 pairs of asteroids suspected to share a common origin, and we mainly consider the primary object of these systems. Finally, the general population, encompassing all known asteroids for which reliable data on their dynamics and composition are available.

In order to construct the largest possible dataset, we included information from a plethora of sources. Using the `rocks`[1] interface for SsODNet[2] (Berthier et al. 2022), we gathered values for physical and dynamical parameters of all asteroids considered in this study with full traceability to their original sources, which are outlined in Appendix A.

The list of binary asteroid systems we consider was sourced from Johnston (2019) and complemented with updates from the Website[3] of the same author and notices from the Central Bureau for Astronomical Telegrams (CBETs)[4]. The list of pairs was extracted from the recent literature (Vokrouhlický & Nesvorný 2008, 2009; Pravec & Vokrouhlický 2009; Kyrylenko et al. 2021; Pravec et al. 2019, 2010; Vokrouhlický et al. 2017, 2022; Žižka et al. 2016; Rożek et al. 2011; Holt et al. 2020; Moskovitz et al. 2019; Kuznetsov et al. 2020).

---

[1] https://rocks.readthedocs.io/
[2] https://ssp.imcce.fr/webservices/ssodnet/
[3] https://www.johnstonsarchive.net/astro/asteroidmoons.html
[4] http://www.cbat.eps.harvard.edu/cbet/RecentCBETs.html

Table 1. Taxonomic classes grouped as complexes (Σ), with their average albedo from objects in the spectroscopic set, and the number of binaries (N_b) and pairs (N_p) considered here.

Classes	Σ	p_V	N_b	N_p
S	S	0.24	121	76
Q	Q	0.29	10	3
V	V	0.27	24	13
C, Ch, B, D, P, Z	C	0.05	14	14
E	E	0.52	5	1
K, L, M	M	0.17	12	3

From the 402 total binaries and 239 pairs, a subset of 279 binaries and 220 pairs were selected that were likely candidates for formation through the YORP spin mechanism. Two criteria were used for the selection of these objects: first, we chose systems for which the diameter of the primary $d_p < 15$ km, and from these we selected systems with a semi-major axis $a < 2.502$ au for binaries or $a < 2.825$ au for pairs, corresponding to objects within the 3:1 and 5:2 mean-motion resonances with Jupiter. The first criterion excludes larger systems, which are unlikely to have formed via the YORP spin mechanism (Polishook et al. 2011). The second limits the set to NEA, Mars-crossing (MC), Hungaria, inner main belt (IMB), and middle main belt (MMB) populations. These dynamical populations contain the vast majority of small binary systems ($d_p < 15$ km), as a result of efficient targeted surveys (e.g., Warner & Stephens 2022; Warner 2015; Warner & Harris 2012). Additionally, these objects are less likely to be influenced by the incompleteness bias found in the outer main belt (OMB; Marsset et al. 2022), and are closer to the Sun, meaning they are in a position to be strongly influenced by the YORP effect (Vokrouhlický et al. 2015). Objects without a known diameter were not rejected from the set, but the diameter of these objects was instead estimated as described in Sect. 3.

No selection was performed based on the spin period of the primary. While theoretical models (Walsh et al. 2008; Jacobson & Scheeres 2011) suggest that these systems are formed through rapid rotation, the spin of the primary may have been reduced because of loss of angular momentum during the formation of the secondary, or through decelerating YORP effects (Pravec et al. 2010). Furthermore, easily accessible datasets of spin periods are typically incomplete, and while early reviews of binary systems and binary candidates (Pravec et al. 2006) listed typical spin periods of NEA binary systems ranging from 2.2 to 2.8 h, with outliers trailing to 4h, current observations show a much broader range (Warner et al. 2021).

Due to limitations in the size of the binary and pair sets, many taxonomic classes are represented by a low number of systems, such as the Ch, L, and E classes. This is compounded when separating the samples by dynamical class. In order to reduce the effects of statistical uncertainties presented by this, in some instances, objects are grouped using a taxonomic classification, where multiple classes are combined (similarly to Mahlke et al. 2021). This is detailed in Table 1. Any objects with a subclass were classified according to their designated primary, meaning that an asteroid classified as Sl would be considered to be of S-type. This is motivated by understandings of known compositional similarities between these classes, such as those highlighted by Vernazza & Beck (2016) or Mahlke et al. (2022).

Although Q-type asteroids are similar in composition to S-type asteroids (Binzel et al. 2001; Nakamura et al. 2011), they
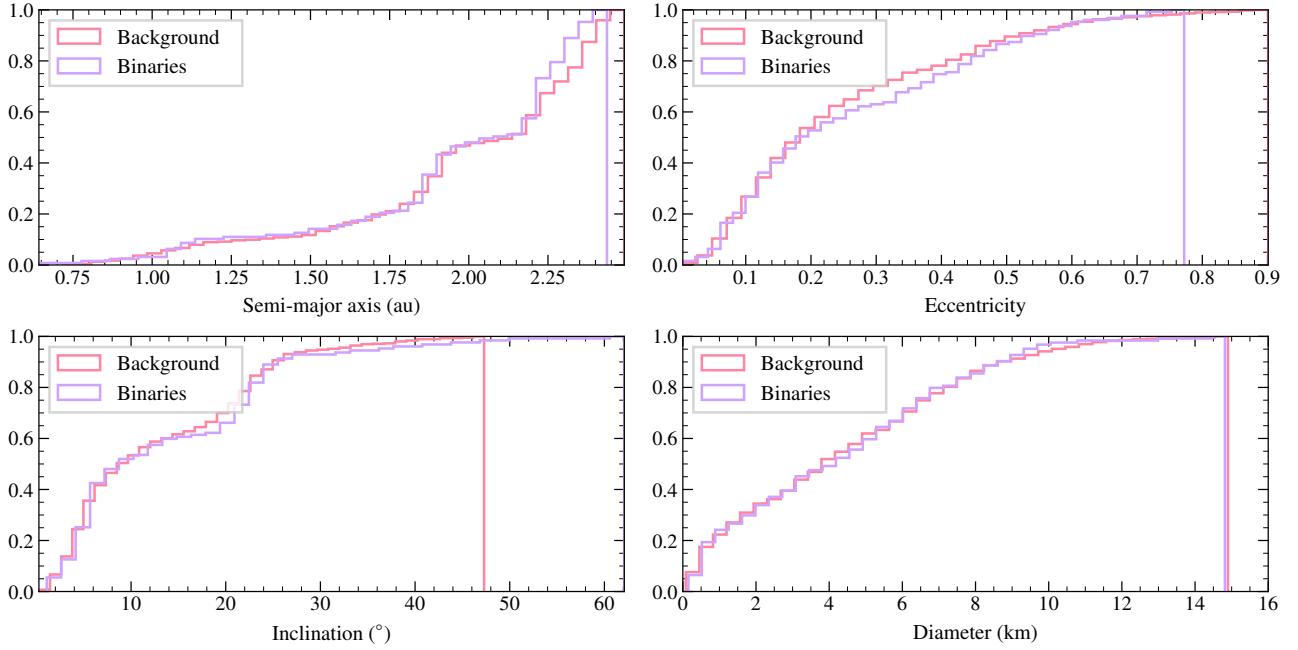
Fig. 2. Cumulative distributions of the semi-major axis, inclination, eccentricity, and diameter of the binary systems (violet) and the selected reference population (red).

are accounted for separately in the reduced taxonomic classification because of the previously observed overabundance of Q-type binary and pair systems (Polishook et al. 2014). While separating objects by dynamical class could reduce some observational biases, doing so is not practical given the current sample size of binary systems. Instead, a reference sample is selected using the methods described in Sect. 3.

3. Reference population

The selection of an appropriate reference population is essential to understanding the surface composition of binary asteroids. As a number of observational biases affect the current sample of known binaries, we aim to mimic this population in order to minimize the effects of such biases.

We consider four parameters in the creation of this set; semi-major axis (a), eccentricity (e), inclination (i), and effective diameter (D). These parameters are considered for the following reasons. We include the orbital elements (a, e, i), as it is well known that there is substantial taxonomic variation as a function of these elements (Gradie & Tedesco 1982; Carvano et al. 2010). The taxonomic distribution of asteroids also shows a substantial dependence on diameter, even when dynamically similar (DeMeo & Carry 2014). Selection across these parameters minimizes potential biases caused by the over-representation of low-mass binaries in the population, as well as observational biases from the ease in observing brighter taxonomic types (Stuart & Binzel 2004; Marsset et al. 2022).

Of the 279 binaries and 220 pairs considered in the present study, estimates of their effective diameters are available for 220 binaries and 65 pair primaries. We estimate the missing effective diameters (D) from the asteroid absolute magnitude H and the average albedo p_V of their taxonomic class (Table 1) using Eq. (1), (Bowell et al. 1989):

$$D = \frac{1329}{\sqrt{p_V}} 10^{-0.2H}. \qquad (1)$$

We build the reference set as follows, considering as an example the set of known binary asteroids for which taxonomy from spectra are available. We create a four-dimensional partition in (a, e, i, D) for the set of binaries. For each object in a box of this partition of space, M objects were then randomly selected with replacement for the reference set from the total population of asteroids within the same variable space. As such, the distribution of selected objects mimics the properties of the binary systems. M is an integer value selected to maximize the size of the reference population while maintaining a reasonable number of instances of object duplication, which naturally occurs in boxes with little taxonomic characterisation.

Figure 2 presents a comparison of the properties of the carefully selected reference population with the binary asteroids. The two distributions are extremely similar. This suggests that this method is effective in selecting a reference sample with excellent dynamical similarity to the set of binary systems, therefore reducing the effects of observational biases present in the set of binary asteroids.

Figure 3 compares the carefully selected reference sample using the partitioning method described here with simpler selections. Most notably, there is a substantially higher abundance of C-class asteroids in the general population of asteroids with spectra than the carefully selected background. This discrepancy is slightly alleviated when a restriction on the semi-major axis of the background population is imposed, but there is still a strong statistical disagreement. A similar disagreement can be seen in the S class. These discrepancies are due to the nonrandom distribution of asteroid taxonomic classes in the asteroid belt. This has been known for decades (Gradie & Tedesco 1982), with a higher abundance of primitive types (C/P/D) in the outer belt than in the inner portions of the belt. More recently, it has also been shown that the relative importance of taxonomic classes is not constant with diameter (DeMeo & Carry 2013, 2014; Bourdelle de Micas et al. 2022). This demonstrates that it is essential to select an appropriate reference population in order to minimize the effects of observational biases affecting both the binary and general populations.
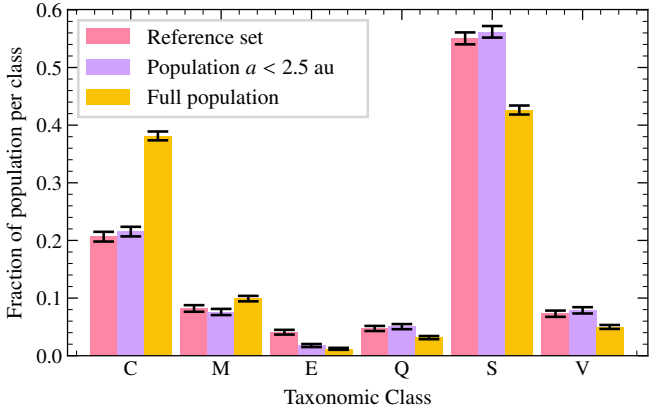
Fig. 3. Illustration of the selection effects on the taxonomic distribution of asteroids. The reference set used hereafter is compared to the entire population of asteroids with taxonomy from spectroscopy, and those whose semi-major axis is less than 2.5 au.

To select an appropriate value of M, it is important to understand the possibility of duplication in the reference sample. Certain areas of the 4D (a, e, i, D) space are significantly emptier than others. Notably, this includes most of the areas in which NEAs are found, which means that these zones are at high risk of excessive duplication when randomly selecting objects in these zones. This could potentially cause significant biases in the reference set, increasing the likelihood of over-including binaries in the reference, and also leading to extreme over-representation of unusual taxonomic classes that may be present in the space. Because of this, the grid used to build the reference sample cannot be arbitrarily small, and M cannot be arbitrarily large. However, a large reference sample is ideal to minimize statistical uncertainties, and so a small value of M is also undesirable. We examined the duplication rates occurring with several values of M and different partitionings, and ultimately determined that a value of $M = 20$ and boxes of 0.28 au, 0.2, 10.0°, and 1.5 km in (a, e, i, D) provides a reasonable balance between duplication and sample size for this set.

The distribution of duplicated objects is not homogeneous within dynamical classes. This is largely due to the high prevalence of binary systems within the near-Earth space, and the low percentage of asteroids belonging to that population. This inconsistency could cause a bias towards taxonomic types prevalent amongst NEAs, such as S- and Q-type asteroids. However, the populations with duplicates and without duplicates show a similar taxonomic distribution, as can be seen in Fig. 4, suggesting that the bias from the anisotropy of the duplicates is not substantially affecting the distribution of classes. Amongst NEAs, where we see the most duplication, the largest discrepancies between the set with duplicates included and the set with duplicates excluded occur in the C and V complexes. Nevertheless, all taxonomic classes show agreement between the sets far below the 1σ level.

To minimize the effects of the inconsistency between different taxonomic schemes, the set of binaries was divided into subsets: those with spectroscopic classifications and those with photometric classifications. Subset membership is mutually exclusive. A separate background population was selected for each of these subsets using the process described above. A similar division was made for the set of asteroid pairs – considering the taxonomy of the primary of the pair – for a total of four subsets and four corresponding reference populations (Table 2). The set membership of asteroids is indicated in Appendix A.
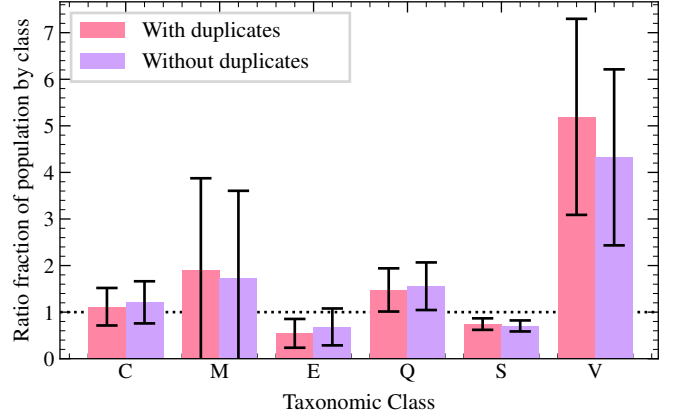
Fig. 4. Ratio of binary systems to the reference sample amongst NEAs in the spectroscopic set when either allowing for duplicates or removing them. The results appear robust against duplication.

Table 2. M values for the selection of the four reference populations.

Population	Technique	M
Binaries	Spectroscopy	20
Binaries	Photometry	30
Pairs	Spectroscopy	15
Pairs	Photometry	100

4. Results

4.1. Spectroscopic set

For objects in the spectroscopic set, we only considered those for which a taxonomy has been derived following the method of Mahlke et al. (2022). The methodology used in this classification is more technically nuanced than previous studies, and accounts for both visible and near-infrared spectra. This classification also accounts for albedo when available, providing another dimension of information that is not considered in the most recent spectroscopic taxonomies (Bus & Binzel 2002; DeMeo et al. 2009). Most objects with known spectra are included in this classification. However, spectra are currently available for only a few thousand objects[5], severely limiting the available reference population of this set. As known binary systems are particularly well represented in the spectroscopic set due to targeted studies by Pajuelo et al. (2018), this set is comparatively more complete, with 127 out of 279 binary systems represented. Pairs are poorly included, with only 36 out of 220 pairs represented (Polishook et al. 2014; Duddy et al. 2013). We compute the relative incidence of binaries and pairs in the general population by taking the ratio between their taxonomic distribution and that of the reference sample.

We estimate the uncertainties from the statistical error in set membership, as follows:

$$\sigma = \sqrt{\frac{p(1-p)}{n}}, \tag{2}$$

where σ is the statistical uncertainty, p is the percentage of the set that a given population occupies, and n is the total number

---

[5] Excluding the recent publication of *Gaia* DR3 visible spectra of 60 000 asteroids (Gaia Collaboration 2023).
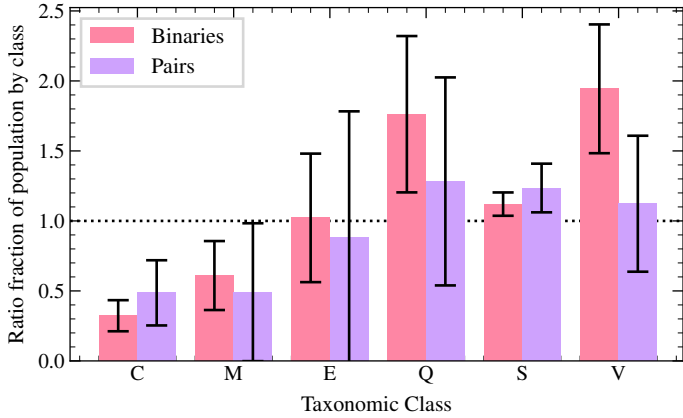
Fig. 5. Taxonomic distribution of binary asteroids relative to the general population, as measured from spectroscopy. A ratio below one indicates an under-representation of the class among binaries, while a ratio above one implies that the class is more represented among binaries.

of objects in the set. Standard-error-propagation techniques then provide the uncertainty in the ratios:

$$\sigma_r = \left|\frac{x}{y}\right| \sqrt{\left(\frac{\sigma_x}{x}\right)^2 + \left(\frac{\sigma_y}{y}\right)^2}, \tag{3}$$

where σ_r is the statistical uncertainty on the ratio, x represents the percentages associated with the population of either binaries or pairs, and y represents the percentages associated with the corresponding background population.

The results of this analysis can be seen in Fig. 5. There is a significant over-representation of Q and V complex asteroids amongst binary systems, and a significant under-representation of C and M complex asteroids. Amongst pairs, we find a significant under-representation of C and M complex asteroids as well, and a marginal over representation of S types.

An additional notable finding within this set is the extremely high prevalence of binary systems amongst V-type NEAs, with $25 \pm 8\%$ of known V types with associated spectra being known binary systems (7 out of a total of 28). While in agreement with the expected total fraction of binary systems amongst NEAs ($15 \pm 4\%$, Pravec et al. 2006), this number is unexpectedly high considering the fact that there have been no obvious campaigns to search for binary systems amongst this population and that there is no reason to assume completeness of the true set of binary systems amongst the currently known population, especially considering the recent discovery of a satellite orbiting V-type (7889) 1994 LX in September 2022.

As visible in Table 3, these binaries were discovered by different researchers, both from radar and light-curve measurements. As little to no information is available on objects that have been similarly investigated, it is difficult to verify how many V-type NEAs have been searched for satellites without detection. Some of these objects were specifically targeted for spectroscopic studies due to their status as binary systems (such as (348400) 2005 JF21, targeted by Pajuelo et al. 2018). Still, the high fraction of binary systems that are V types, combined with the high fraction of V-type NEAs that are known binaries, suggests that there is a striking correlation between the two.

4.2. Photometric set

While spectroscopic classification is highly consistent and more nuanced than other methods of taxonomy, the availability of

Table 3. Discovery information for V-type binary NEAs.

Asteroid	Year	Technique	PI
(7889) 1994 LX	2022	LC	Warner
(68063) 2000 YJ66	2014	LC	Warner
(164121) 2003 YT1	2004	Radar	Nolan
(348400) 2005 JF21	2015	Radar	Stephens
(357439) 2004 BL86	2015	LC	Pollock
(450894) 2008 BT18	2008	Radar	Benner
(523775) 2014 YB35	2015	Radar	Naidu

Notes. Asteroid name and number (Asteroid), year of announcement (Year), discovery technique (Technique), either light curve (LC) or radar (Radar), and primary investigator of the discovery (PI).
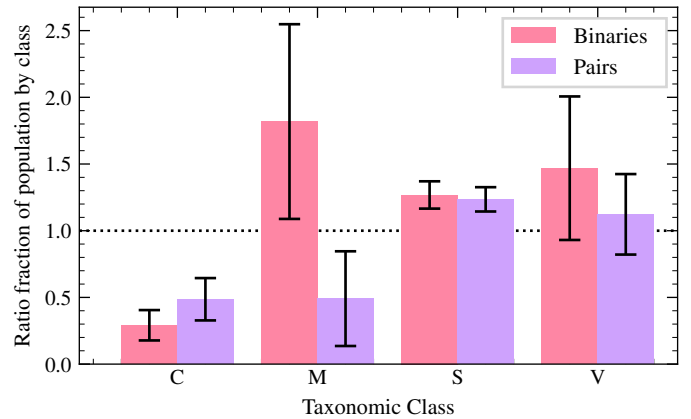

Fig. 6. Taxonomic distribution of binary asteroids relative to the general population, as measured from photometry. Q types are merged with S types in most photometric studies, and are therefore not separately available.

asteroid spectra severely limits its reach. Although photometric classification schemes can be inconsistent, the number of objects with a photometric classification is significantly larger than that of those with a spectroscopic classification, with recent photometric studies such as Popescu et al. (2018), Sergeyev & Carry (2021), and Sergeyev et al. (2022) containing over 200 000 objects, while the spectroscopic set of Mahlke et al. (2022) contains only around 4000 asteroids. As such, a much larger number of binary and pair systems have been classified in this manner. Because of this, we study these objects using the technique described for the spectroscopic set; see Fig. 6.

We find a significant under-representation of C complex asteroids amongst binary systems, a significant over-representation of S types, and a slight over-representation of M complex asteroids, which are dominated by L-type asteroids[6]. We find similar results amongst the pairs, with an additional under-representation of M complex asteroids.

5. Discussion

The results presented in Figs. 5 and 6 point to strong differences in the abundances of taxonomic types amongst binary systems compared to the reference population. We considered the C complex (encompassing classes C, B, P, and D) asteroids to be primitive because of their opaque-rich surface composition, which is a characteristic they share with inter-planetary

---

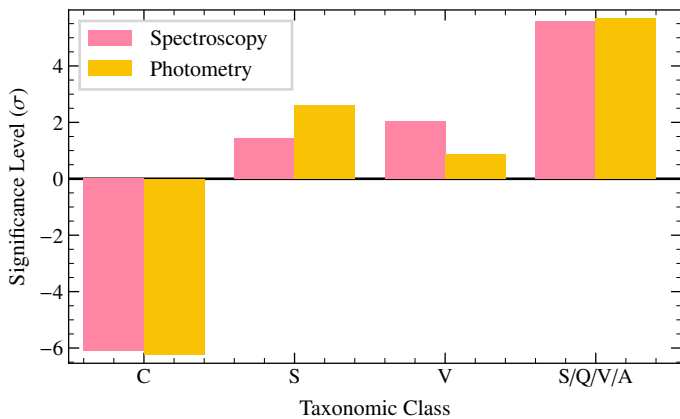[6] In this case, the M complex contains no M-type asteroids.

Fig. 7. Number of standard deviations away from the background for selected reduced taxonomic classes, with a negative value representing classes with lower representation in the specified population than the background, and a positive value representing a higher representation in the specified population than the background. Classes are ordered from least to most thermally evolved moving from left to right, with the most substantial under-representation in the C complex, and the most substantial over-representation in the V class and S/Q/V/A complex.

dust particles (Vernazza et al. 2015, IDPs). Although P types share spectral similarities with E-, M-, and X-type asteroids, and as such are often associated together as an X complex (Bus & Binzel 2002; DeMeo et al. 2009), these do not represent true similarities in composition, and are therefore irrelevant for the purposes of this study. These objects also share characteristics with other remnants of the early Solar System, such as comets (Elkins-Tanton & Weiss 2017). We consider an additional super-complex of mafic-silicate-rich asteroids belonging to S, Q, V, and A, as there is evidence for substantial heating in their formation history in the geological history of meteorite analogues (McCord et al. 1970; Vernazza et al. 2014). K, L, M, and X classes were not included in either category as these objects are of ambiguous origin (CO/CV and iron meteorites have been proposed as analogs; e.g., Sunshine et al. 2008; Ockert-Bell et al. 2010; Eschrig et al. 2021), and are not substantially opaque or mafic-silicate rich. X-type asteroids encompass objects with no known albedo that could belong to the E, M, or P classes, all of which have similar spectral properties but very different compositions (Bus & Binzel 2002; DeMeo et al. 2009; Vernazza et al. 2015; Mahlke et al. 2022). M-type asteroids have been found to be metal rich, implying that they are from thermally differentiated parent bodies; however, some members of this class have been found to have signatures of silicates or hydration, making the origin of these asteroids ambiguous (Rivkin et al. 2000; Mahlke et al. 2022).

We compared the relative abundances of asteroids in these categories for the binaries and pairs with respect to their corresponding background populations. For the spectroscopic set, there was an underabundance of 6.1σ for primitive-type asteroids, and an overabundance of 5.6σ for S/Q/V/A-type asteroids, suggesting that there is a strong preference for binary formation amongst S-, Q-, V- and A-type asteroids with respect to primitive-type asteroids.

Furthermore, from analysis of the reduced taxonomic classes (Fig. 5), it seems that the more thermally evolved the parent body of an asteroid, the more likely it is to form a binary system. This trend can be seen in Fig. 7, where the clear increase in the number of standard deviations away from agreement with the background can be seen as the taxonomic

groups become increasingly thermally evolved. There is a strong underabundance in the C complex, which contains primitive IDPs, and a strong overabundance of V-type binary systems, which are associated with the fully differentiated parent body (4) Vesta. This increase is seen across both the photometric and spectroscopic sets.

These findings are in alignment with recent theoretical models based on Hayabusa2 and OSIRIS-REx data by Zhang et al. (2022), which suggest that rapidly rotating asteroids with primitive compositions are more likely to undergo internal deformation than to form binary systems. Our compilation of taxonomic classes for binary systems and creation of a reference population supports these theoretical predictions.

6. Conclusions

By collecting the taxonomic class for 279 binary asteroids with SsODNet (Berthier et al. 2022), we find significant observational evidence for a nonrandom distribution of binary systems amongst taxonomic classes. There is an over-representation of multiple asteroids amongst mafic-silicate-rich types (Q, V, A, E) and under-representation amongst primitive opaque-rich types (C, B, P, D). The high representation of binary systems amongst V-type NEAs also suggests that objects forming from further differentiated parent bodies may be more likely to form binaries, but limited sample size prevents us from making any robust conclusions. While taxonomies from spectra are valued more highly in this study due to the availability of a low-error, highly consistent data set from Mahlke et al. (2022), taxonomies from photometric measurements provide similar results. The taxonomies of 220 asteroid pairs were also considered, based on the primary body of the pairs, and we find that this taxonomic distribution is consistent with that found in the set of binary systems. This is in alignment with recent predictions by Zhang et al. (2022). The consistency between the distributions of binaries and pairs implies that low-albedo taxonomic types have difficulty forming binary systems rather than difficulty maintaining them.

References

Alí-Lagoa, V., & Delbo', M. 2017, A&A, 603, A55
Berthier, J., Carry, B., Mahlke, M., & Normand, J. 2022, ArXiv e-prints [arXiv:2209.10697]
Binzel, R. P., Rivkin, A. S., Bus, S. J., Sunshine, J. M., & Burbine, T. H. 2001, Meteor. Planet. Sci., 36, 1167
Bourdelle de Micas, J., Fornasier, S., Avdellidou, C., et al. 2022, A&A, 665, A83
Bowell, E., Hapke, B., Domingue, D., et al. 1989, Asteroids II (Tucson: University of Arizona Press), 524
Bracewell, R. N., & MacPhie, R. H. 1979, Icarus, 38, 136
Bus, S. J., & Binzel, R. P. 2002, Icarus, 158, 146
Carry, B., Solano, E., Eggl, S., & DeMeo, F. E. 2016, Icarus, 268, 340
Carvano, J. M., Hasselmann, P. H., Lazzaro, D., & Mothé-Diniz, T. 2010, A&A, 510, A43
Chapman, C. R., Veverka, J., Thomas, P. C., et al. 1995, Nature, 374, 783
Delbo, M. 2004, PhD thesis, Free University of Berlin, Germany
DeMeo, F. E., & Carry, B. 2013, Icarus, 226, 723
DeMeo, F. E., & Carry, B. 2014, Nature, 505, 629
DeMeo, F. E., Binzel, R. P., Slivan, S. M., & Bus, S. J. 2009, Icarus, 202, 160
Duddy, S. R., Lowry, S. C., Christou, A., et al. 2013, MNRAS, 429, 63

Elkins-Tanton, L. T., & Weiss, B. P. 2017, Planetesimals: Early Differentiation and Consequences for Planets (Cambridge: Cambridge University Press)
Eschrig, J., Bonal, L., Beck, P., & Prestgard, T. J. 2021, Icarus, 354, 114034
Fraser, W. C., Bannister, M. T., Pike, R. E., et al. 2017, Nat. Astron., 1, 0088
Fujiwara, A., Kawaguchi, J., Yeomans, D. K., et al. 2006, Science, 312, 1330
Gaia Collaboration (Galluccio, L., et al.) 2023, A&A in press, https://doi.org/10.1051/0004-6361/202243791
Gibbons, G. W. 1971, Nature, 232, 465
Gradie, J., & Tedesco, E. 1982, Science, 216, 1405
Hadley, S. M. 1903, Popular Astron., 11, 240
Hamilton, V. E., Simon, A. A., Christensen, P. R., et al. 2019, Nat. Astron., 3, 332
Herchel, J. S. 1832, MNRAS, 2, 51
Holt, T. R., Vokrouhlický, D., Nesvorný, D., Brož, M., & Horner, J. 2020, MNRAS, 499, 3630
Hung, D., Hanuš, J., Masiero, J. R., & Tholen, D. J. 2022, PSJ, 3, 56
Jacobson, S. A., & Scheeres, D. J. 2011, Icarus, 214, 161
Jacobson, S. A., Scheeres, D. J., & McMahon, J. 2014, ApJ, 780, 60
Johnston, W. R. 2019, NASA Planetary Data System, 4
Kuznetsov, E. D., Rosaev, A. E., Plavalova, E., & Safronova, V. S. 2020, INASAN Sci. Rep., 5, 52
Kyrylenko, I., Krugly, Y. N., & Golubov, O. 2021, A&A, 655, A14
Mahlke, M., Carry, B., & Denneau, L. 2021, Icarus, 354, 114094
Mahlke, M., Carry, B., & Mattei, P. A. 2022, A&A, 665, A26
Mainzer, A., Grav, T., Masiero, J., et al. 2012, ApJ, 760, L12
Mainzer, A., Bauer, J., Grav, T., et al. 2014, ApJ, 784, 110
Margot, J. L., Pravec, P., Taylor, P., Carry, B., & Jacobson, S. 2015, in Asteroids IV (Tucson: University of Arizona Press), 355
Marsset, M., DeMeo, F. E., Burt, B., et al. 2022, AJ, 163, 165
Masiero, J. R., Mainzer, A. K., Grav, T., et al. 2011, ApJ, 741, 68
Masiero, J. R., Mainzer, A. K., Grav, T., et al. 2012, ApJ, 759, L8
Masiero, J. R., Grav, T., Mainzer, A. K., et al. 2014, ApJ, 791, 121
Masiero, J. R., Mainzer, A. K., Bauer, J. M., et al. 2020, PSJ, 1, 5
McCord, T. B., Adams, J. B., & Johnson, T. V. 1970, Science, 168, 1445
Merline, W. J., Weidenschilling, S. J., Durda, D. D., et al. 2002, in Asteroids III (Tucson: University of Arizona Press), 289
Moskovitz, N. A., Fatka, P., Farnocchia, D., et al. 2019, Icarus, 333, 165
Mueller, M., Delbo', M., Hora, J. L., et al. 2011, AJ, 141, 109
Myhrvold, N., Pinchuk, P., & Margot, J.-L. 2022, PSJ, 3, 30
Nakamura, T., Noguchi, T., Tanaka, M., et al. 2011, Science, 333, 1113
Nugent, C. R., Mainzer, A., Masiero, J., et al. 2015, ApJ, 814, 117
Nugent, C. R., Mainzer, A., Bauer, J., et al. 2016, AJ, 152, 63
Ockert-Bell, M. E., Clark, B. E., Shepard, M. K., et al. 2010, Icarus, 210, 674

Pajuelo, M., Birlan, M., Carry, B., et al. 2018, MNRAS, 477, 5590
Polishook, D., Brosch, N., & Prialnik, D. 2011, Icarus, 212, 167
Polishook, D., Moskovitz, N., Binzel, R. P., et al. 2014, Icarus, 233, 9
Popescu, M., Licandro, J., Carvano, J. M., et al. 2018, A&A, 617, A12
Pravec, P., & Vokrouhlický, D. 2009, Icarus, 204, 580
Pravec, P., Scheirich, P., Kušnirák, P., et al. 2006, Icarus, 181, 63
Pravec, P., Vokrouhlický, D., Polishook, D., et al. 2010, Nature, 466, 1085
Pravec, P., Fatka, P., Vokrouhlický, D., et al. 2019, Icarus, 333, 429
Rivkin, A. S., Howell, E. S., Lebofsky, L. A., Clark, B. E., & Britt, D. T. 2000, Icarus, 145, 351
Rožek, A., Breiter, S., & Jopek, T. J. 2011, MNRAS, 412, 987
Sergeyev, A. V., & Carry, B. 2021, A&A, 652, A59
Sergeyev, A. V., Carry, B., Onken, C. A., et al. 2022, A&A, 658, A109
Stuart, J. S., & Binzel, R. P. 2004, Icarus, 170, 295
Sunshine, J. M., Connolly, H. C., McCoy, T. J., Bus, S. J., & La Croix, L. M. 2008, Science, 320, 514
Taylor, M. B. 2005, ASP Conf. Ser., 347, 29
Trilling, D. E., Mueller, M., Hora, J. L., et al. 2010, AJ, 140, 770
Trilling, D. E., Mommert, M., Hora, J., et al. 2016, AJ, 152, 172
Usui, F., Kuroda, D., Müller, T. G., et al. 2011, PASJ, 63, 1117
Vernazza, P., & Beck, P. 2016, Planetesimals: Early Differentiation and Consequences for Planets, eds. L. T. Elkins-Tanton, & B. P. Weiss (Cambridge: Cambridge University Press)
Vernazza, P., Zanda, B., Binzel, R. P., et al. 2014, ApJ, 791, 120
Vernazza, P., Marsset, M., Beck, P., et al. 2015, ApJ, 806, 204
Vokrouhlický, D., & Nesvorný, D. 2008, AJ, 136, 280
Vokrouhlický, D., & Nesvorný, D. 2009, AJ, 137, 111
Vokrouhlický, D., Bottke, W. F., Chesley, S. R., Scheeres, D. J., & Statler, T. S. 2015, in Asteroids IV (Tucson: University of Arizona Press), 509
Vokrouhlický, D., Pravec, P., Ďurech, J., et al. 2017, AJ, 153, 270
Vokrouhlický, D., Fatka, P., Micheli, M., Pravec, P., & Christensen, E. J. 2022, A&A, 664, L17
Walsh, K. J., Richardson, D. C., & Michel, P. 2008, Nature, 454, 188
Warner, B. D. 2015, Minor Planet Bull., 42, 132
Warner, B. D., & Harris, A. 2012, AAS/Div. Planet. Sci. Meeting Abstracts, 44, 110.15
Warner, B. D., & Stephens, R. D. 2022, Minor Planet Bull., 49, 223
Warner, B. D., Harris, A. W., & Pravec, P. 2021, NASA Planetary Data System, 10
Weidenschilling, S. J., Paolicchi, P., & Zappala, V. 1989, in Asteroids II, eds. R. P. Binzel, T. Gehrels, & M. S. Matthews (Tucson: University of Arizona Press), 643
Zhang, Y., Michel, P., Barnouin, O. S., et al. 2022, Nat. Commun., 13, 4589
Žižka, J., Galád, A., Vokrouhlický, D., et al. 2016, A&A, 595, A20

Appendix A: Compiled parameters

The majority of data considered in this study were sourced from SsODNet (Berthier et al. 2022), which contains a compilation of many independent studies. The exact parameters and objects considered in this study are available electronically at CDS. The first 12 lines of each set are included in this Appendix A. Column headings are as follows, 'Number' (asteroid number), 'Name' (asteroid name), 'D' (primary diameter, if available), 'σ_D' (uncertainty in primary diameter, if available), 'D ref' (reference corresponding to primary diameter, if available), 'p_V' (albedo, if available), 'σ_{p_V}' (uncertainty in albedo, if available), 'Tax. method' (method for taxonomy, either spectroscopy (spec) or photometry (phot)), 'Tax. scheme' (taxonomic scheme), 'Class' (taxonomic class), 'Waverange' (waverange over which the taxonomy is determined), 'Tax. Ref' (reference for the determination of the objects taxonomy). All albedo values are sourced from Berthier et al. (2022), who computed albedo from most-recent absolute magnitudes and best-estimates of diameter using Equation 1.

Table A.1. Parameters of included objects in the spectroscopic binaries set, first 12 lines included.

Number	Name	D	σ_D	D Ref.	p_V	σ_{p_V}	Tax. method	Tax. scheme	Class	Waverange	Tax. Ref.
1016	Anitra	9.98	0.07	Masiero et al. (2011)	0.3	0.18	Spec	Mahlke	S	VISNIR	Mahlke et al. (2022)
1798	Watts	6.88	0.09	Masiero et al. (2012)	0.24	0.19	Spec	Mahlke	S	VISNIR	Mahlke et al. (2022)
2491	Tvashtri	3.13	0.09	Myhrvold et al. (2022)	0.7	0.19	Spec	Mahlke	A	VISNIR	Mahlke et al. (2022)
2881	Meiden	5.84	0.07	Masiero et al. (2014)	0.27	0.19	Spec	Mahlke	S	VISNIR	Mahlke et al. (2022)
3122	Florence	4.4	0.03	Myhrvold et al. (2022)	0.26	0.18	Spec	Mahlke	S	VISNIR	Mahlke et al. (2022)
3792	Preston	5.13	0.2	Nugent et al. (2016)	0.29	0.2	Spec	Mahlke	S	VISNIR	Mahlke et al. (2022)
4435	Holt	5.56	0.27	Hung et al. (2022)	0.26	0.21	Spec	Mahlke	S	VISNIR	Mahlke et al. (2022)
4666	Dietz	6.73	0.4	Nugent et al. (2016)	0.25	0.22	Spec	Mahlke	A	VISNIR	Mahlke et al. (2022)
7002	Bronshten	3.12	0.31	Alí-Lagoa & Delbo' (2017)	0.2	0.27	Spec	Mahlke	S	VISNIR	Mahlke et al. (2022)
15745	Yuliya	0.77	0.15	Trilling et al. (2010)	0.32	0.44	Spec	Mahlke	S	VISNIR	Mahlke et al. (2022)
190166	2005 UP156	1.04	0.02	Nugent et al. (2015)	0.2	0.19	Spec	Mahlke	S	VISNIR	Mahlke et al. (2022)
226514	2003 UX34	-	-	-	-	-	Spec	Mahlke	S	VISNIR	Mahlke et al. (2022)

Table A.2. Parameters of included objects in the photometric binaries set, first 12 lines included.

Number	Name	D	σ_D	D Ref.	p_V	σ_{pV}	Tax. method	Tax. scheme	Class	Waverange	Tax. Ref.
2602	Moore	-	-	-	-	-	Phot	Bus-DeMeo	S	VIS	DeMeo & Carry (2013)
2883	Barabashov	4.96	0.07	Masiero et al. (2014)	0.32	0.19	Phot	Bus-DeMeo	S	VIS	DeMeo & Carry (2013)
5500	Twilley	4.26	0.11	Myhrvold et al. (2022)	0.3	0.19	Phot	Bus-DeMeo	S	VIS	DeMeo & Carry (2013)
6245	Ikufumi	7.88	0.21	Nugent et al. (2016)	0.13	0.19	Phot	Bus-DeMeo	X	VIS	Sergeyev & Carry (2021)
7393	Luginbuhl	5.43	0.1	Nugent et al. (2015)	0.27	0.19	Phot	Bus-DeMeo	S	NIR	Popescu et al. (2018)
9474	Cassadrury	3.57	0.16	Masiero et al. (2011)	0.24	0.21	Phot	Bus-DeMeo	S	VIS	DeMeo & Carry (2013)
18303	1980 PU	-	-	-	-	-	Phot	Bus-DeMeo	S	VIS	Sergeyev et al. (2022)
20882	Paulsanchez	-	-	-	-	-	Phot	Bus-DeMeo	S	VIS	DeMeo & Carry (2013)
25021	Nischaykumar	2.15	0.52	Masiero et al. (2011)	0.16	0.52	Phot	Bus-DeMeo	L	VIS	Sergeyev et al. (2022)
26420	1999 XL103	-	-	-	-	-	Phot	Bus-DeMeo	V	VIS	Sergeyev & Carry (2021)
72036	2000 XM44	3.1	0.58	Nugent et al. (2016)	0.28	0.42	Phot	Bus-DeMeo	S	VIS	Sergeyev et al. (2022)
250162	2002 TY57	-	-	-	-	-	Phot	Bus-DeMeo	S	VIS	Carry et al. (2016)

Table A.3. Parameters of included objects in the photometric pairs set, first 12 lines included.

Number	Name	D	σ_D	D Ref.	p_V	σ_{pV}	Tax. method	Tax. scheme	Class	Waverange	Tax. Ref.
34380	Pratikvangal	2.2	0.55	Masiero et al. (2011)	0.26	0.53	Phot	Bus-DeMeo	S	VIS	DeMeo & Carry (2013)
38184	1999 KF	2.0	0.37	Masiero et al. (2011)	0.31	0.41	Phot	Bus-DeMeo	S	VIS	DeMeo & Carry (2013)
43008	1999 UD31	-	-	-	-	-	Phot	Bus-DeMeo	S	VIS	Sergeyev et al. (2022)
44620	1999 RS43	-	-	-	-	-	Phot	Bus-DeMeo	S	VIS	Sergeyev et al. (2022)
48652	1995 VB	2.25	0.23	Masiero et al. (2011)	0.23	0.27	Phot	Bus-DeMeo	S	VIS	DeMeo & Carry (2013)
49791	1999 XF31	-	-	-	-	-	Phot	Bus-DeMeo	S	VIS	Sergeyev et al. (2022)
51609	2001 HZ32	1.97	0.67	Masiero et al. (2011)	0.3	0.71	Phot	Bus-DeMeo	V	VIS	Sergeyev et al. (2022)
51866	2001 PH3	3.86	0.12	Nugent et al. (2015)	0.25	0.19	Phot	Bus-DeMeo	S	VIS	Sergeyev et al. (2022)
52478	1995 TO	-	-	-	-	-	Phot	Bus	S	VIS	Carvano et al. (2010)
55764	1992 DG12	-	-	-	-	-	Phot	Bus-DeMeo	A	VIS	Sergeyev et al. (2022)
55913	1998 FL12	-	-	-	-	-	Phot	Bus-DeMeo	X	VIS	Sergeyev et al. (2022)
56700	2000 LL28	-	-	-	-	-	Phot	Bus-DeMeo	S	VIS	DeMeo & Carry (2013)

Table A.4. Parameters of included objects in the spectroscopic pairs set, first 12 lines included.

Number	Name	D	σ_D	D Ref.	p_V	σ_{pv}	Tax. method	Tax. scheme	Class	Waverange	Tax. Ref.
42946	1999 TU95	4.75	0.1	Masiero et al. (2011)	0.2	0.19	Spec	Mahlke	S	VISNIR	Mahlke et al. (2022)
52852	1998 RB75	2.53	0.38	Masiero et al. (2011)	0.27	0.35	Spec	Mahlke	V	VISNIR	Mahlke et al. (2022)
53537	Zhangyun	-	-	-	-	-	Spec	Mahlke	S	VISNIR	Mahlke et al. (2022)
54041	2000 GQ113	2.68	0.73	Masiero et al. (2011)	0.28	0.57	Spec	Mahlke	V	VISNIR	Mahlke et al. (2022)
54827	Kurpfalz	2.09	0.54	Masiero et al. (2011)	0.24	0.55	Spec	Mahlke	Q	VISNIR	Mahlke et al. (2022)
63440	Rozek	-	-	-	-	-	Spec	Mahlke	C	VISNIR	Mahlke et al. (2022)
74096	1998 QD15	-	-	-	-	-	Spec	Mahlke	S	VISNIR	Mahlke et al. (2022)
88604	2001 QH293	5.8	0.13	Masiero et al. (2011)	0.2	0.19	Spec	Mahlke	S	VISNIR	Mahlke et al. (2022)
92652	2000 QX36	-	-	-	-	-	Spec	Mahlke	S	VISNIR	Mahlke et al. (2022)
101703	1999 CA150	-	-	-	-	-	Spec	Mahlke	S	VISNIR	Mahlke et al. (2022)

Table A.5. Parameters of included objects in the photometric binaries reference set, first 12 lines included.

Number	Name	D	σ_D	D Ref.	p_V	σ_{pv}	Tax. method	Tax. scheme	Class	Waverange	Tax. Ref.
26920	1996 TQ12	1.52	0.2	Masiero et al. (2011)	0.42	0.33	Phot	Bus-DeMeo	Q	VIS	Sergeyev & Carry (2021)
30577	2001 OU103	1.7	0.2	Masiero et al. (2011)	0.27	0.29	Phot	Bus-DeMeo	S	VIS	Sergeyev et al. (2022)
30958	1994 TV3	1.93	0.1	Masiero et al. (2011)	0.63	0.21	Phot	Bus-DeMeo	C	VIS	DeMeo & Carry (2013)
53428	1999 TD2	-	-	-	-	-	Phot	Bus-DeMeo	X	VIS	Sergeyev et al. (2022)
53440	1999 XQ33	-	-	-	-	-	Phot	Bus	A	VIS	Carvano et al. (2010)
55913	1998 FL12	-	-	-	-	-	Phot	Bus-DeMeo	X	VIS	Sergeyev et al. (2022)
63260	2001 CN	-	-	-	-	-	Phot	Bus-DeMeo	X	VIS	Sergeyev & Carry (2021)
74590	1999 OG2	-	-	-	-	-	Phot	Bus-DeMeo	S	VIS	Sergeyev et al. (2022)
82074	2000 YE119	2.69	0.19	Masiero et al. (2011)	0.22	0.23	Phot	Bus-DeMeo	S	VIS	DeMeo & Carry (2013)
85563	1998 BF7	-	-	-	-	-	Phot	Bus-DeMeo	X	VIS	DeMeo & Carry (2013)
90216	2003 AS85	-	-	-	-	-	Phot	Bus-DeMeo	L	VIS	Sergeyev et al. (2022)
92036	1999 VZ180	-	-	-	-	-	Phot	Bus-DeMeo	X	VIS	Sergeyev & Carry (2021)

Table A.6. Parameters of included objects in the spectroscopic binaries reference set, first 12 lines included.

Number	Name	D	σ_D	D Ref.	p_V	σ_{pv}	Tax. method	Tax. scheme	Class	Waverange	Tax. Ref.
4581	Asclepius	-	-	-	-	-	Spec	Mahlke	X	VISNIR	Mahlke et al. (2022)
33342	1998 WT24	0.4	0.06	Delbo (2004)	0.67	0.35	Spec	Mahlke	K	VISNIR	Mahlke et al. (2022)
88254	2001 FM129	0.8	0.01	Mainzer et al. (2014)	0.22	0.19	Spec	Mahlke	Q	VISNIR	Mahlke et al. (2022)
138971	2001 CB21	0.34	0.01	Usui et al. (2011)	0.58	0.2	Spec	Mahlke	S	VISNIR	Mahlke et al. (2022)
152563	1992 BF	0.37	0.1	Mainzer et al. (2012)	0.16	0.56	Spec	Mahlke	K	VISNIR	Mahlke et al. (2022)
164202	2004 EW	0.16	0.03	Mueller et al. (2011)	0.31	0.37	Spec	Mahlke	E	VISNIR	Mahlke et al. (2022)
208023	1999 AQ10	0.15	0.04	Trilling et al. (2016)	0.5	0.56	Spec	Mahlke	S	VISNIR	Mahlke et al. (2022)
281375	2008 JV19	-	-	-	-	-	Spec	Mahlke	X	VISNIR	Mahlke et al. (2022)
310442	2000 CH59	-	-	-	-	-	Spec	Mahlke	Q	VISNIR	Mahlke et al. (2022)
401885	2001 RV17	-	-	-	-	-	Spec	Mahlke	S	VISNIR	Mahlke et al. (2022)
474163	1999 SO5	-	-	-	-	-	Spec	Mahlke	S	VISNIR	Mahlke et al. (2022)
518810	2010 CF19	0.08	0.01	Mainzer et al. (2014)	0.47	0.23	Spec	Mahlke	S	VISNIR	Mahlke et al. (2022)

Table A.7. Parameters of included objects in the photometric pairs reference set, first 12 lines included.

Number	Name	D	σ_D	D Ref.	p_V	σ_{pv}	Tax. method	Tax. scheme	Class	Waverange	Tax. Ref.
163678	2002 XT65	-	-	-	-	-	Phot	Bus-DeMeo	X	VIS	Sergeyev & Carry (2021)
177647	2004 RF110	-	-	-	-	-	Phot	Bus-DeMeo	S	VIS	Sergeyev et al. (2022)
182310	2001 OO43	-	-	-	-	-	Phot	Bus-DeMeo	X	VIS	Sergeyev & Carry (2021)
191919	2005 QS157	-	-	-	-	-	Phot	Bus-DeMeo	S	VIS	DeMeo & Carry (2013)
194922	2002 AK125	-	-	-	-	-	Phot	Bus-DeMeo	B	VIS	Sergeyev et al. (2022)
218019	2001 YX14	-	-	-	-	-	Phot	Bus-DeMeo	S	VIS	Sergeyev et al. (2022)
258019	2001 FY138	-	-	-	-	-	Phot	Bus-DeMeo	S	VIS	Sergeyev et al. (2022)
471448	2011 UZ145	-	-	-	-	-	Phot	Bus-DeMeo	C	VIS	Sergeyev et al. (2022)
475868	2007 CZ12	-	-	-	-	-	Phot	Bus-DeMeo	X	VIS	Sergeyev et al. (2022)
482128	2010 RY1	-	-	-	-	-	Phot	Bus-DeMeo	V	VIS	Sergeyev et al. (2022)
503415	2016 DC2	-	-	-	-	-	Phot	Bus-DeMeo	X	VIS	Sergeyev & Carry (2021)
514044	2014 MM50	-	-	-	-	-	Phot	Bus-DeMeo	X	VIS	Sergeyev & Carry (2021)

Table A.8. Parameters of included objects in the spectroscopic pairs reference set, first 12 lines included.

Number	Name	D	σ_D	D Ref.	p_V	σ_{p_V}	Tax. method	Tax. scheme	Class	Waverange	Tax. Ref.
1920	Sarmiento	2.85	0.16	Masiero et al. (2011)	0.51	0.22	Spec	Mahlke	E	VISNIR	Mahlke et al. (2022)
4736	Johnwood	2.72	0.07	Myhrvold et al. (2022)	0.78	0.19	Spec	Mahlke	E	VISNIR	Mahlke et al. (2022)
6461	Adam	2.6	0.47	Nugent et al. (2016)	0.43	0.41	Spec	Mahlke	E	VISNIR	Mahlke et al. (2022)
7829	Jaroff	2.73	0.16	Masiero et al. (2011)	0.44	0.22	Spec	Mahlke	E	VISNIR	Mahlke et al. (2022)
15692	1984 RA	1.72	0.32	Masiero et al. (2011)	0.58	0.41	Spec	Mahlke	E	VISNIR	Mahlke et al. (2022)
16585	1992 QR	2.0	0.29	Masiero et al. (2011)	0.57	0.35	Spec	Mahlke	E	VISNIR	Mahlke et al. (2022)
20043	Ellenmacarthur	-	-	-	-	-	Spec	Mahlke	S	VISNIR	Mahlke et al. (2022)
25884	Asai	1.91	0.46	Masiero et al. (2011)	0.6	0.52	Spec	Mahlke	E	VISNIR	Mahlke et al. (2022)
53424	1999 SC3	-	-	-	-	-	Spec	Mahlke	S	VISNIR	Mahlke et al. (2022)
138970	2001 CV19	1.09	0.11	Alí-Lagoa & Delbo' (2017)	0.28	0.27	Spec	Mahlke	S	VISNIR	Mahlke et al. (2022)
230269	2001 XZ6	-	-	-	-	-	Spec	Mahlke	S	VISNIR	Mahlke et al. (2022)
275611	1999 XX262	1.48	0.01	Masiero et al. (2020)	0.04	0.18	Spec	Mahlke	Ch	VISNIR	Mahlke et al. (2022)